Application of Independent Joint Control Strategy for Discrete-Time Servo Control of Overhead Cranes

Arash Khatamianfar, and Mehdi Bagheri

Abstract

In this study, a new servo control system is presented for the overhead crane based on discrete-time state feedback approach. It provides both robust tracking and load swing suppression. Inspired from independent joint and computed torque control in robot manipulator field, a new model is derived in which the crane actuators are considered as the main plant. The crane nonlinearities are then treated as disturbances acting on each actuator and being compensated via feed forward control. The load swing control is integrated to the servo controller through modifying the reference trolley acceleration. The stability of the tracking error and swing dynamics are proven based on error dynamic equation and passivity theory. Experimental results indicate the high performance and great potential for industrial application of the proposed control system.

Keywords—Discrete-time control; independent joint control; overhead crane; servo control.

I. INTRODUCTION

Over the past two decades, automatic control of over-head cranes, which play a pivotal role in transportation industry, has become an intriguing research topic due to its challenging control behavior as it requires fast and accurate load positioning for higher efficiency as well as restraining load swings for safety. Load hoisting during trolley acceleration exacerbates load swings, and being underactuated makes it even harder to suppress them. Many efforts have been done to address these challenges such as the use of linearized model with linear control algorithms in [1]–[3] and recently in [4], [5]. More sophisticated control algorithms, however, have been re-ported to tackle crane nonlinearities including nonlinear coupling control [6], [7], Nonlinear tracking control [8], [9], adaptive control [10], [11], sliding mode control [12], [13], and fuzzy logic-based control [14], [15]. Most recently, the application of nonlinear model predictive control (MPC) on overhead crane has also been proposed [16], [17]. Moreover, visual-based control for overhead crane has been applied in [18]. However, from practical aspects and implementation point of view, designing a control system for an overhead crane explicitly in discrete-time would be more beneficial in regards to discretization errors and sampling time issues compared to complex and nonlinear control algorithms in continuous-time. So far, only in [19] discrete-time integral sliding mode control was reported to be used on an overhead crane with a linearized model for set-point control.

To meet the two main objectives in automatic control of the overhead crane, namely, high performance trajectory tracking with robust load swing damping, a new servo control system based on discrete-time state feedback is proposed. We motivated by the idea of independent joint control for robot manipulators [20] in which the actuators of the overhead crane are considered as the main plant. The coupling effects, mainly caused by nonlinear mechanical dynamics, are treated as disturbances. Since these nonlinear dynamics are known in advance, they can be compensated through feed forward action (known as computed torque control [21]). However, applying this method on crane is challenging since the swing dynamics is not directly involved in the decoupled model. Nevertheless, we managed to solve this issue by adopting and improving the idea firstly proposed by Lee in [22] where the trolley acceleration can be modified to control load swings. Therefore, our proposed servo control system is comprised of five parts: a reference model for generating the desired state trajectories; an observer to estimate system states; a feed forward signal generator for providing ideal output response and disturbance rejection; a feedback action to reduce the tracking error, and finally the load swing control based on swing dynamics for robust swing damping. Unlike many previous works where rope length is assumed to be constant or varying slowly, our proposed servo control system is capable of handling high speed load hoisting as well as swing stability and high performance trajectory tracking, even in repetitive motions, as one of the main contributions of this study. Discrete-time nature of the controller design, however, makes it easier to be implemented in any digital processors. Furthermore, the design procedure is much simpler with a new decoupled model. The results are supported by mathematical proof and experimental validation.

The rest is organized as follows. The overhead

Manuscript received October 30, 2014; revised December 29, 2014; accepted January 18, 2015.

A. Khatamianfar, School of Electrical Engineering and Telecommunications, The University of New South Wales, Sydney, NSW 2052, Australia (e-mails: a.khatamianfar@unsw.edu.au).

M. Bagheri, School of Electrical Engineering and Telecommunications, The University of New South Wales, Sydney, NSW 2052, Australia (e-mails: m.bagheri@unsw.edu.au).

crane modeling is explained in Section II. Details of the proposed servo control system design are described in Section III. Section IV covers the stability analysis of the proposed servo control system, followed by the design of reference trajectories. The practical results and evaluation are provided in Section V, and finally the paper is concluded in Section VI.

II. Overhead Crane Modeling

A. Dynamic Model of an Overhead Crane

By the assumption that the mass and stiffness of the hoisting rope are neglected and the load mass is considered as a point mass, the equations of motion for an overhead crane, as shown in Fig. 1, are given as follows [23]:

$$(m_x+m)\ddot{x}+mlC_\theta\ddot{\theta}+mS_\theta\ddot{l}+D_x\dot{x}+2mC_\theta\dot{l}\dot{\theta}-mlS_\theta\dot{\theta}^2=f_x, \quad (1)$$

$$(m_l+m)\ddot{l}+mS_\theta\ddot{x}+D_l\dot{l}-ml\dot{\theta}^2-mgC_\theta=f_l, \quad (2)$$

$$ml^2\ddot{\theta}+mlC_\theta\ddot{x}+2ml\dot{l}\dot{\theta}+mglS_\theta=0, \quad (3)$$

where S_θ and C_θ denote $sin\theta$ and $cos\theta$, respectively; x, l, and θ are the trolley position, hoisting rope length, and swing angle, respectively; m is the load mass; m_x and m_l are the x (traveling) and l (hoisting) components of the crane mass, respectively, which contain the equivalent masses of rotating parts such as motors and their drive trains; D_x and D_l denote viscous damping coefficients associated with x and l motions, respectively; f_x and f_l are the driving forces in x and l directions, respectively, and g is gravitational acceleration. The load swing dynamics given in (3), and subsequently (1), can be simplified as below:

$$(m_x+mS_\theta^2)\ddot{x}+mS_\theta\ddot{l}+D_x\dot{x}-mlS_\theta\dot{\theta}^2-mgC_\theta S_\theta=f_x, \quad (4)$$

$$(m_l+m)\ddot{l}+mS_\theta\ddot{x}+D_l\dot{l}-ml\dot{\theta}^2-mgC_\theta=f_l, \quad (5)$$

$$l\ddot{\theta}+C_\theta\ddot{x}+2\dot{l}\dot{\theta}+gS_\theta=0. \quad (6)$$

In this study, we propose a dynamic model in which the actuators (permanent magnet DC motors) are the main plant to be controlled. The nonlinear dynamics of the overhead crane (coupling effects due to x and l motions) are then considered as load disturbances acting on the corresponding actuator as in independent joint control strategy [20], which is a common practice in the field of robot manipulator control. Therefore, the proposed system model is given as follows [24]:

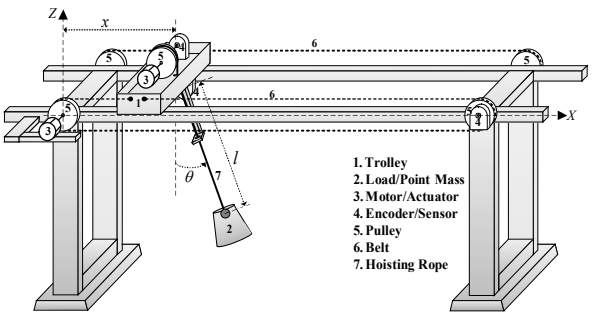

Fig. 1. Schematic structure of an overhead crane with its actuators.

$$J_{ex}\ddot{x}+B_{ex}\dot{x}=K_{ex}v_{ax}-f_{dx}, \quad (7)$$

$$J_{el}\ddot{l}+B_{el}\dot{l}=K_{el}v_{al}-f_{dl}, \quad (8)$$

where J_{ex} and J_{el} are the total effective moment of inertia of motor shaft, gear box and pulleys that are moving the trolley (J_{mx}) and hoisting the crane load (J_{ml}), respectively, which include the effects of m_x and m_l as well, i.e., $J_{ex}=J_{mx}/r_{gx}R_{px}+ r_{gx}R_{px}m_x$ and $J_{el}=J_{ml}/r_{gl}R_{pl}+ r_{gl}R_{pl}m_l$ (r_g is the gear box ratio and R_p is the pulley radius); B_{ex} and B_{el} are the total damping effects of traveling (B_{mx}) and hoisting (B_{ml}) motors, respectively, which include the effects of D_x and D_l as well, i.e., $B_{ex}=B_{mx}/r_{gx}R_{px}+r_{gx}R_{px}D_x$ and $B_{el}=B_{ml}/r_{gl}R_{pl}+r_{gl}R_{pl}D_l$; v_{ax} and v_{al} are input control voltages for traveling and hoisting motors, respectively; K_{ex} and K_{el} are the ratios of motor torque constant and motor winding resistances that convert input voltages to driving forces for traveling and hoisting motors, respectively; f_{dx} and f_{dl} are the load disturbances on traveling and hoisting motors, respectively, which are generated from crane dynamics given in (4) and (5) without the linear terms plus the coulomb friction effects acting on traveling (f_{cfx}) and hoisting (f_{cfl}) motions, i.e., $f_{dx}=r_{gx}R_{px}(f_x-m_x\ddot{x}-D_x\dot{x})+f_{cfx}$ and $f_{dl}=r_{gl}R_{pl}(f_l-m_l\ddot{l}-D_l\dot{l}+f_{cfl})$.

B. Discrete-Time Form of an Overhead Crane Model

Since the continuous-time model of the overhead crane obtained in (7) and (8) has type-I for both traveling and hoisting subsystems and it is already in linear form, we can discretize the model as follows:

$$v_x(z)=\frac{b_{1x}}{z-a_{1x}}v_{ax}(z)-\frac{b_{d1x}}{z-a_{1x}}f_{dx}(z), \quad (9.a)$$

$$x(z)=\frac{T_s}{z-1}v_x(z), \quad (9.b)$$

$$v_l(z)=\frac{b_{1l}}{z-a_{1l}}v_{al}(z)-\frac{b_{d1l}}{z-a_{1l}}f_{dl}(z), \quad (10.a)$$

$$l(z)=\frac{T_s}{z-1}v_l(z), \quad (10.b)$$

where v_x and v_l are the traveling and hoisting velocities, respectively; a_{1x}, b_{1x}, b_{d1x}, a_{1l}, b_{1l}, and b_{d1l} are the discrete-time transfer function coefficients (all positive) obtained using methods given in [25], and T_s is the sampling time. Thus, the proposed discrete-time state space form of the overhead crane model can be obtained by choosing the state variables as $[x_1(k)\ x_2(k)\ x_3(k)\ x_4(k)]^T=[x(k)\ v_x(k)\ l(k)\ v_l(k)]^T$ and the output as

the measurements of x and l, i.e., $[y_1(k)\ y_2(k)]^T = [x(k)\ l(k)]^T$, as follows:

$$\begin{aligned} \boldsymbol{x}(k+1) &= A\boldsymbol{x}(k) + B\boldsymbol{u}(k) + W_d \boldsymbol{f}_d(k), \\ \boldsymbol{y}(k) &= C\boldsymbol{x}(k), \end{aligned} \tag{11}$$

where $\boldsymbol{x}(k)$ is the vector of state variables, $\boldsymbol{u}(k) = [v_{ax}(k)\ v_{al}(k)]^T$ is the control input vector; $\boldsymbol{f}_d(k) = [f_{dx}(k)\ f_{dl}(k)]^T$ is the vector of input disturbances; A=*BlockDiag*$\{A_x,\ A_l\}$ is the system matrix; B=*BlockDiag*$\{B_x,\ B_l\}$ is the control input matrix; C=*BlockDiag*$\{C_x,\ C_l\}$ is the output matrix, and W_d=*BlockDiag*$\{W_{dx},\ W_{dl}\}$ is the input disturbance matrix. *BlockDiag*$\{.\}$ is a notation used for block-diagonal matrix and the inner matrices are given as follows:

$$A_i = \begin{bmatrix} 1 & T_s \\ 0 & a_{1i} \end{bmatrix},\ B_i = \begin{bmatrix} 0 \\ b_{1i} \end{bmatrix},\ W_{di} = \begin{bmatrix} 0 \\ -b_{d1i} \end{bmatrix},\ C_i = \begin{bmatrix} 1 & 0 \end{bmatrix}, \quad \text{for } i = x, l. \tag{12}$$

Although the swing dynamics is not explicitly incorporated in the proposed model, it is indirectly included in trolley dynamics in (4) to form traveling motion disturbance f_{dx}. However, a new robust swing damping control law based on swing dynamics in (5) will be developed and then integrated with our proposed servo control system.

III. Proposed Servo Control System Design

A. Servo Control System Structure

The block diagram of the proposed servo control system is illustrated in Fig. 2 It consists of a reference model that generates the desired state trajectories, an observer that estimates the system states and reduces the effects of input and measurement noises, a feed forward signal generator that gives the desired output response when applied to the open-loop system which also includes load disturbance attenuation (using the idea of computed torque control), a feedback action to decrease the tracking error, and finally the load swing control to suppress load swings through modifying traveling reference acceleration. Thus, the servo control law is given as follows:

$$\begin{aligned} \boldsymbol{u}(k) &= \boldsymbol{u}_{fb}(k) + \boldsymbol{u}_{ff}(k) \\ &= K(\boldsymbol{x}_{rm}(k) - \hat{\boldsymbol{x}}(k)) + \boldsymbol{u}_{ff}(k), \end{aligned} \tag{13}$$

where K=*BlockDiag*$\{K_x,\ K_l\}$ is the feedback gain; $\boldsymbol{x}_{rm}(k) = [\boldsymbol{x}_{rmx}(k)\ \boldsymbol{x}_{rml}(k)]^T = [x_{rmx1}(k)\ x_{rmx2}(k)\ x_{rml1}(k)\ x_{rml2}(k)]^T = [x_r(k) v_{xr}(k)\ l_r(k)\ v_{lr}(k)]^T$ is the reference state trajectory vector; $\hat{\boldsymbol{x}}(k)$ is the estimates of states; $\boldsymbol{u}_{fb}(k)$ is the feedback control action, and $\boldsymbol{u}_{ff}(k) = [u_{ffx}(k)\ u_{ffl}(k)]^T$ is the feed forward signal.

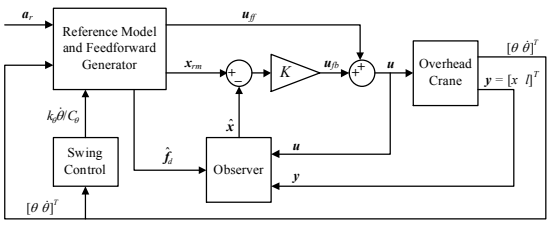

Fig. 2. The block diagram of the proposed servo control system.

The reference model for generating $\boldsymbol{x}_{rm}$ is designed as the combination of two discrete-time integrators for traveling and hoisting motions as in (9.b) and (10.b), respectively, which can be modeled in a state space form as below:

$$\begin{aligned} \boldsymbol{x}_{rm}(k+1) &= A_m \boldsymbol{x}_{rm}(k) + B_m \boldsymbol{u}_c(k), \\ \boldsymbol{y}_{rm}(k) &= C_m \boldsymbol{x}_{rm}(k), \end{aligned} \tag{14}$$

where $\boldsymbol{u}_c(k) = [u_{cx}(k)\ u_{cl}(k)]^T$ is the command signal vector considered to be the reference traveling and hoisting accelerations, i.e., $\boldsymbol{a}_r(k) = [a_{xr}(k)\ a_{lr}(k)]^T$; $\boldsymbol{y}_{rm}(k) = [x_r(k)\ l_r(k)]^T$ is the reference output response; A_m=*BlockDiag*$\{A_{mx},\ A_{ml}\}$, B_m=*BlockDiag*$\{B_{rx},\ B_{rl}\}$, and C_m=*BlockDiag*$\{C_{rx},\ C_{rl}\}$ are the reference model system matrix, input matrix, and output matrix, respectively, with inner matrices given as follows:

$$A_{mi} = \begin{bmatrix} 1 & T_s \\ 0 & 1 \end{bmatrix},\ B_{mi} = \begin{bmatrix} 0 \\ T_s \end{bmatrix},\ C_{mi} = \begin{bmatrix} 1 & 0 \end{bmatrix}, \quad \text{for } i = x, l. \tag{15}$$

The state estimates are provided by the observer dynamic equations given as follows:

$$\begin{aligned} \hat{\boldsymbol{x}}(k+1) = {} & A\hat{\boldsymbol{x}}(k) + B\boldsymbol{u}(k) + W_d \hat{\boldsymbol{f}}_d(k) \\ & + L(\boldsymbol{y}(k) - C\hat{\boldsymbol{x}}(k)), \end{aligned} \tag{16}$$

where L=*BlockDiag*$\{L_x,\ L_l\}$ is the observer gain, and $\hat{\boldsymbol{f}}_d(k) = [\hat{f}_{dx}(k)\ \hat{f}_{dl}(k)]^T$ is the computed disturbance vector calculated using (4), (5), the measurements of θ, $\dot{\theta}$, $\boldsymbol{u}_c$, reference trajectories, and coulomb friction model given by [26]:

$$f_{cfi}(v_i) = \begin{cases} \alpha_{1i} & v_i > 0 \\ -\alpha_{2i} & v_i < 0 \end{cases}, \quad \text{for } i = x, l, \tag{17}$$

where α_{1i} and α_{2i} are coulomb friction constants in positive and negative directions, respectively.

B. Feed forward Signal Generation

Given the proposed servo control law in (13), a main question is how to design the feed forward signal $\boldsymbol{u}_{ff}$. The answer lies in the fact that the DC motor velocity has the same pattern as its input voltage. Therefore, based on the definition of $\boldsymbol{u}_{ff}$, we can use reference traveling and hoisting velocities (x_{rmx2}, x_{rml2}) and the transfer functions relating input voltages to velocities given in (9.a) and (10.a) to find open-loop control inputs. Thus, we can write the following difference equation:

$$\begin{aligned} x_{rmi2}(k+1) = {} & a_{1i} x_{rmi2}(k) + b_{1i} u_{ffi}(k) + b_{d1i} \hat{f}_{di}(k), \\ & \text{for } i = x, l. \end{aligned} \tag{18}$$

According to the reference model given in (14) and (15) we also have $x_{rmi2}(k+1) = x_{rmi2}(k) + T_s u_{ci}(k)$, which helps us to generate the feed forward signal using the reference model by substituting $x_{rmi2}(k+1)$ in (18) leading to the following:

$$\boldsymbol{u}_{ff}(k) = \Phi_{ff}\boldsymbol{x}_{rm}(k) + \Gamma_{ff}\boldsymbol{u}_c(k) + \Lambda_{ff}\hat{\boldsymbol{f}}_d(k), \tag{19}$$

where $\Phi_{ff} = BlockDiag\{\Phi_x, \Phi_l\}$; $\Gamma_{ff} = BlockDiag\{\gamma_x, \gamma_l\}$; $\Lambda_{ff} = BlockDiag\{\lambda_x, \lambda_l\}$, with inner matrices given as below:

$$\Phi_i = \begin{bmatrix} 0 & \dfrac{1-a_{i1}}{b_{i1}} \end{bmatrix},\ \gamma_i = \frac{T_s}{b_{i1}},\ \lambda_i = \frac{b_{di1}}{b_{i1}},\ \text{for}\ \ i = x, l. \tag{20}$$

It can be seen from (18) and (19) that the effects of overhead crane nonlinearities are compensated through computation of $\hat{\boldsymbol{f}}_d(k)$ at each sampling time and including them in $\boldsymbol{u}_{ff}(k)$.

IV. Stability and Robustness Analysis of the Proposed Servo Control System

We can establish the stability analysis of the proposed servo control system in the following theorem:

Proposition: Suppose that $\mathbf{a}_r$ and $\mathbf{x}_{rm}$ are uniformly bounded and $l > 0$ for all time $k \geq 0$. Then, the proposed servo control law with the observer dynamics in (13) and (16), respectively, guarantee that:

1. Swing dynamics is finite-gain L_2 stable, i.e., $\|\theta, \dot{\theta}\| \leq \varepsilon_2 < \infty$ as $k \to \infty$,
2. Tracking error is uniformly bounded, i.e., $\|\mathbf{x}_{rm} - \mathbf{x}\| \leq \varepsilon_1 < \infty$, for all $k \geq 0$, if and only if:

i. $|\theta(0)| < \pi/2$ and $\mathbf{a}_r(k) = 0$ for $kT_s \geq t_f$ with some $t_f < \infty$,
ii. The matrices K and L are chosen such that (A-BK) and (A-LC) are stable,
iii. The model uncertainty is uniformly bounded, i.e., $\|\hat{\mathbf{f}}_d - \mathbf{f}_d\| \leq c_1 < \infty$,
iv. $u_{cx} = a_{xr} + k_\theta \dot{\theta}/C_\theta$ *with* $k_\theta \geq 1.5|v_l|_{max}$,

where t_f *is the final time of the trajectory,* c_1 *is a positive constant, and* k_θ *is the load swing control gain.*

Proof 1. Recall from swing dynamics in (6). The following positive definite function can be considered as a candidate Lyapunov function:

$$V_\theta = \frac{1}{2} l\dot{\theta}^2 + g(1 - C_\theta). \tag{21}$$

Taking time-derivative of V_θ and substituting $l\ddot{\theta}$ from (6) results in the following:

$$\dot{V}_\theta = -C_\theta \dot{\theta}\ddot{x} - 1.5\dot{l}\dot{\theta}^2. \tag{22}$$

As we require that trolley acceleration follows the reference traveling acceleration which results in $x \to x_r$ and $v_x \to v_{xr}$, it is a true assumption that $\ddot{x}$ would eventually follow u_{cx}. Thus, applying $u_{cx} = a_{xr} + k_\theta \dot{\theta}/C_\theta$ for $\ddot{x}$, we can write $\dot{V}_\theta$ as follows:

$$\dot{V}_\theta = -C_\theta \dot{\theta} a_{xr} - (k_\theta + 1.5\dot{l})\dot{\theta}^2, \tag{23}$$

$$\dot{V}_\theta \leq \dot{\theta} a_{xr} - (k_\theta + 1.5v_l)\dot{\theta}^2. \tag{24}$$

Deploying the passivity-based control theory [27], it can be seen that by considering a_{rx} as input to swing dynamics $(u), \dot{\theta}$ as output (y), and choosing $k_\theta \geq 1.5|v_l|_{max}$, the swing dynamics in (6) becomes output strictly passive with V_θ as the storage function, and subsequently finite-gain L_2 stable (i.e., bounded -input bounded-output stable for square integrable signals) since we can write (24) as below:

$$\begin{aligned} &\dot{\theta} a_{xr} \geq \dot{V}_\theta + (k_\theta + 1.5v_l)\dot{\theta}^2. \\ &uy \geq \dot{V}_\theta + y\varphi(y),\ \ \varphi(y) = (k_\theta + 1.5v_l)\dot{\theta} \Rightarrow\ y\varphi(y) > 0. \end{aligned} \tag{25}$$

Remark: Based on the concept of passivity theory, there should be a swing damping action during load transportation to suppress and stabilize load swings. Since the overhead crane is an underactuated system, there is no direct control input for load swing. Our proposed swing control acts as a swing friction force exerted indirectly into the system via modifying a_{xr} at each sampling time, where $\dot{\theta}$ is obtained computationally using backward difference of the swing angle measurement θ.

Proof 2. Define $\boldsymbol{e} = \boldsymbol{x}_{rm} - \boldsymbol{x}$ as the tracking error and $\hat{\boldsymbol{e}} = \boldsymbol{x} - \hat{\boldsymbol{x}}$ as the state estimation error. Subtracting (14) from (11) gives the error dynamic equation as follows:

$$\begin{aligned} \boldsymbol{e}(k+1) = {} & A_m \boldsymbol{x}_{rm}(k) - A\boldsymbol{x}(k) + B_m \boldsymbol{u}_c(k) \\ & - B\boldsymbol{u}(k) - W_d \boldsymbol{f}_d(k). \end{aligned} \tag{26}$$

Now, substituting $\boldsymbol{u}$ and $\boldsymbol{u}_{ff}$ from (13) and (19), respectively, leads to the following:

$$\begin{aligned} \boldsymbol{e}(k+1) = {} & (A_m - B\Phi_{ff})\boldsymbol{x}_{rm}(k) - A\boldsymbol{x}(k) - BK\boldsymbol{e}(k) - BK\hat{\boldsymbol{e}}(k) \\ & + (B_m - B\Gamma_{ff})\boldsymbol{u}_c(k) - B\Lambda_{ff}\hat{\boldsymbol{f}}_d(k) - W_d \boldsymbol{f}_d(k). \end{aligned} \tag{27}$$

Recall from all inner matrices in (12), (15), and (20) and the fact that all matrices are in block diagonal form. The error dynamic equation given above is then simplified since $A_m - B\Phi_{ff} = A$, $B_m = B\Gamma_{ff}$, and $B\Lambda_{ff} = -W_d$, as follows:

$$\begin{aligned} \boldsymbol{e}(k+1) = {} & (A - BK)\boldsymbol{e}(k) - BK\hat{\boldsymbol{e}}(k) \\ & + W_d(\hat{\boldsymbol{f}}_d(k) - \boldsymbol{f}_d(k)). \end{aligned} \tag{28}$$

We can now find the solution of the error dynamic equation assuming that $\boldsymbol{e}(0) = 0$ as below:

$$\begin{aligned} \boldsymbol{e}(k) = {} & \sum_{j=0}^{k-1} \Phi_{cl}(k-1-j)(W_d(\hat{\boldsymbol{f}}_d(j) - \boldsymbol{f}_d(j)) \\ & - BK\hat{\boldsymbol{e}}(j)), \end{aligned} \tag{29}$$

where $\Phi_{cl}(k) = (A-BK)^k$ is the closed-loop transition matrix. Based on the conditions given in *ii.* and *iii.* in the theorem, it is well established that the response of the tracking error to the uniformly bounded excitations (i.e.,$\hat{\boldsymbol{e}}$and $\hat{\boldsymbol{f}}_d - \boldsymbol{f}_d$) is uniformly bounded for all $k \geq 0$ [28] since we have

$$\|\sum_{j=0}^{k-1}\Phi_{cl}(k-1-j)\| \leq c_2 < \infty, \quad \text{and} \quad \|\hat{\boldsymbol{e}}(k)\| \leq c_3 < \infty. \tag{30}$$

Therefore, the following proposition is hold:

$$\begin{aligned} &\|\boldsymbol{e}(k)\| = \|\sum_{j=0}^{k-1}\Phi_{cl}(k-1-j)(W_d(\hat{\boldsymbol{f}}_d(j) - \boldsymbol{f}_d(j)) - BK\hat{\boldsymbol{e}}(j))\| \\ &\|\boldsymbol{e}(k)\| \leq c_4(c_1) + c_4(c_3) \leq \varepsilon \leq \infty \end{aligned} \tag{31}$$

Where c_2-c_4 are various positive constants. It can be also shown that the state estimation error is uniformly bounded similar to the given proof, and in this case, the model uncertainty serves as the uniformly bounded excitation to estimation error dynamics. We can find state estimation error equation as follows:

$$\hat{\boldsymbol{e}}(k+1) = (A-LC)\hat{\boldsymbol{e}}(k) - W_d(\hat{\boldsymbol{f}}_d(k) - \boldsymbol{f}_d(k)). \tag{32}$$

Remark: As is proven, the proposed servo control system is capable of robustly track the reference trajectories with uniformly bounded tracking error. However, the reference traveling trajectory ($\boldsymbol{x}_{rmx}$) would slightly differ from the original designed one at the end of the trajectory since the reference model is taking integral from the modified traveling reference acceleration (u_{cx}) rather than the original one (a_{xr}). The amount of deviation created in $\boldsymbol{x}_{rmx}$ will depend on the amount of initial load swing and how fast it is being suppressed. This problem could be easily solved in the design of reference trajectories explained in the following section.

A. Reference Trajectory Planning

In practice, overhead cranes are usually operated along a typical anti-swing trajectory in which the crane is first accelerated until it reaches a normal velocity and the load is mostly hoisted up (accelerating zone). Then, the crane is moved at a normal velocity with no load hoisting (constant velocity zone), and finally it is decelerated to the destination with load being hoisted down (decelerating zone). Thus, the required reference trajectory profiles for traveling and hoisting motions are designed as shown in Fi.3 using the so-called linear segments with parabolic blends or LSBP for short [20]. To solve the problem of deviation in $\boldsymbol{x}_{rmx}$, especially for final trolley position x_{rmx1}, a time interval (t_p) is added after the crane reaches its final point at t_f for fine tuning of the trolley position. Within this period, no swing damping control is needed as load swings have been suppressed before t_f, and thus, any deviation in $\boldsymbol{x}_{rmx}$ can be corrected. The procedure is summarized as follows:

TABLE I
EXPERIMENTAL OVERHEAD CRANE SETUP PARAMETERS

Parameters	J_{ei} (kg/m^2)	B_{ei}(N.m.s/rad)	r_{gi}	R_{pi} (m)	K_{ei} (N.m/Amp.Ω)	α_{1i}	α_{2i}
Traveling	75e−4	96.3e−3	13e−3	37.5e−3	14e−4	23e−4	21e−4
Hoisting	66e−4	24.55e−2	13e−3	13.5e−3	14e−4	13e−4	14e−4

TABLE III
REFERNCE TRAJECTORY PARAMETERS

Parameters	a_i (m/sec^2)	v_{mi} (m/sec)	$x_{rmi1}(0)$ (m)	$x_{rmi1}(t_f)$ (m)	t_b (sec)	t_f (sec)	t_p (sec)
Traveling	22.5e−3	9e−2	5e−2	50e−2	4	9	5
Hoisting	50e−3	10e−2	25e−2	5e−2	4	9	5

*Step*1: Find the correction velocity (v_{xrc}) required to move trolley from deviated final reference position (x_{rmfd}) to the original designed one (x_{rmf}) within $t_p/2$seconds at time t_f, i.e., $v_{xrc} = 2(x_{rmf} - x_{rmfd})/t_p$.

*Step*2: Set the initial conditions of the traveling reference model to $[v_{xrc} x_{rmfd}]^T$ at time t_f.

*Step*3: Reset the initial condition of v_{xr} to zero at time $t_f + t_p/2$.

*Step*4: Continue tracking for a further $t_p/2$ seconds to finish position tuning at $t_f + t_p$.

It should be noted that in all three zones of crane operation load swing damping is active and it suppresses the swings quickly which leads to $k_\theta \dot{\theta} / C_\theta \rightarrow 0$. Thus, the deviation in $\boldsymbol{x}_{rmx}$ is not considerable and t_p can be chosen as short as possible.

V. PRACTICAL RESULTS

A. Experimental Overhead Crane Setup

The laboratory-sized overhead crane setup used in this study, as shown in Fig. 4, is manufactured by the INTECO Limited [29]. This setup is driven by 24V PM DC motors. The measurements are made by identical position encoders with the resolution of 4069 pulses per rotation.

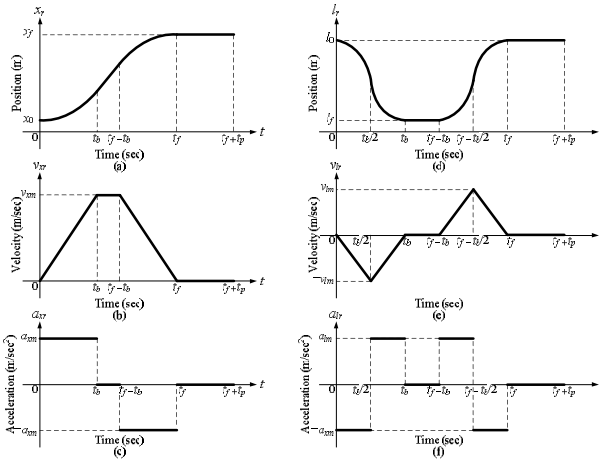

Fig. 3. LSPB trajectories: (a) Position profile, (b) Velocity profile, and (c) Acceleration profile for traveling motion; (d) Position profile, (e) Velocity profile, and (f) Acceleration profile for hoisting motion

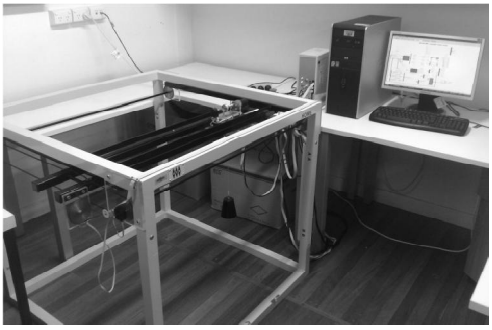

Fig. 4. The experimental overhead crane setup used in this study.

The setup is equipped with RT-DAC/PCI9030 multipurpose digital I/O board connected to a power interface board and installed on a personal computer (Intel® Core2Due 3.00GHz CPU with 3GB RAM). This setup works with the sampling time Ts = 0.01sec and all functions of the board are accessible form a Toolbox provided by the manufacturer and operates in MATLAB® environment.

B. Experimental Results and Validation

The overhead crane model parameters required for the design of the proposed servo control system are given in Table I with m = 0.8kg which is assumed to be known, and g = 9.81m/sec2. The reference trajectories for both traveling and hoisting motions are designed taking into account the maximum admissible torque and speed of the DC motors and the setup workspace limits. The designed values are given in TABLE I. The feedback gain matrix K is calculated using robust pole-placement techniques given in [30] which accounts for perturbations in the pair (A, B), i.e., $eig\ (A\text{-}BK) = [0.62\ 0.88\ 0.73\ 0.74]^T$,. The observer gain L is obtained by using Kalman filter method such that the observer dynamics are faster than the close-loop dynamics. The load swing control gain is chosen as k_θ=0.2 to satisfy *iv.* in the theorem since $|v_l|_{max}$= 0.1m/sec.

The experimental results are shown in Fig. 5-8. Since repeatability is an important factor in any industrial control system [20], we designed the trajectory to begin from a starting point and then return back after reaching the destination. The proposed servo control system was run for four times consecutively and the position tracking is plotted in Fig. 5(a), with control input voltages in Fig. 5(b) which are bounded within the range of ±24V. As can be seen, the experiment shows a high performance with robust tracking for both traveling and hoisting motions. The estimated states are also depicted in Fig. 6(a) and 6(b) indicating the stable operation of the observer. To illustrate the precision of the tracking, the zoomed-in views for the extended period of t_p at the end of each trajectory are shown in Fig. 7. The servo controller was able to bring back the trolley position to the original destination with high accuracy after being slightly deviated caused by swing control.

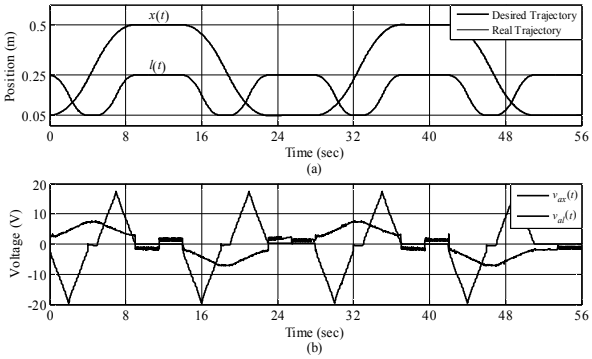

Fig. 5. (a) Desires and real trajectories for traveling and hoisting motions with load swing control, (b) Control input voltages with swing control.

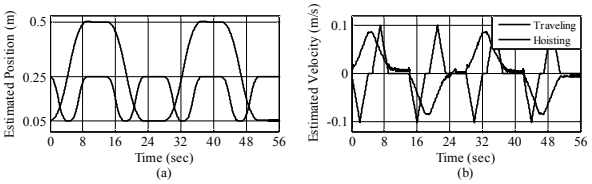

Fig. 6. Estimated states: (a) Position estimates, (b) Velocities estimates.

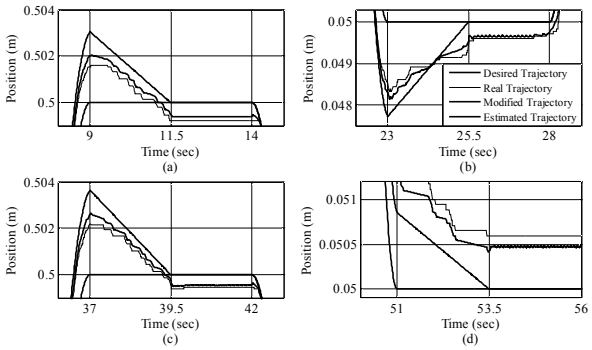

Fig. 7. Zoomed-in view at the end of each trajectory comparing desired, real, modified, and estimated position trajectories: (a) 1st Trajectory, (b) 2nd Trajectory, (c) 3rd Trajectory, (d) 4th Trajectory

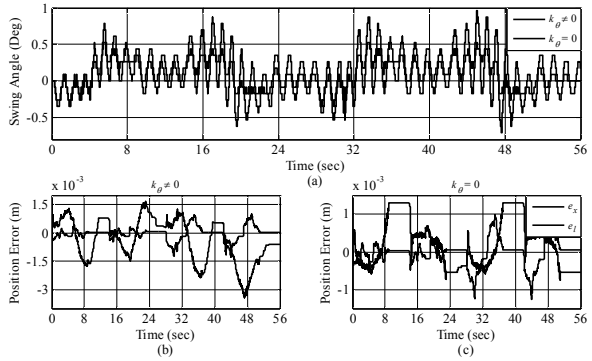

Fig. 8. (a) Load swings with and without swing control action, (b) Tracking error with swing control, (c) Tracking error without swing control.

Nevertheless, the capability of the proposed control system in both damping the load swings and robustly tracking the reference trajectory was further tested

through running the experiment twice–once with load swing control ($k_\theta \neq 0$) and once without it ($k_\theta = 0$). As is shown in Fig. (a), load swings are successfully suppressed when the proposed load swing control is applied alongside the servo controller as opposed to having no swing control where the load swings tend to increase. The position tracking error in both cases are also plotted in Fig. (b) and 8(c) which are robustly bounded with high tracking precision at the end of each trajectory. These experimental results clearly indicate the superiority of the proposed servo control system in both high accuracy load positioning and robust load swing damping. Moreover, the ability to maintain the high performance control during all trajectory repetitions is a significant outcome for practical application of the proposed servo control system for overhead cranes in real world.

VI. CONCLUSION

A new servo control system has been designed and tested on an overhead crane to address the problem of high performance anti-swing tracking control. The control system is based on discrete-time state feedback approach, which is an advantage in terms of practical implementation, and provides accurate load positioning as well as suppressing load swings. To achieve the above-mentioned goals, a new model has been proposed for the overhead crane which considers the crane actuators as the main plant. The nonlinear dynamics of the carne are included in the model as measured disturbance which were compensated via feed forward control. The servo controller was designed using the discretized state space form of the given model which consists of a reference model for generating reference trajectories, an observer to estimate the system states, a feed forward action that generates the desired output response with disturbance attenuation, a feedback action to reduce tracking error, and finally, the load swing control incorporated to the servo controller through modification of the traveling reference acceleration. The load swing control law is designed via passivity-based control. The robustness of both tracking error and load swing dynamics was proven mathematically and the verifying experimental results indicated the superiority of the proposed servo control system, especially for industrial application. The proposed servo control system can be applicable on overhead cranes with AC-type electrical motors since the combined mechanical and electrical equations of an electric motor, either DC-type or AC-type motor, maintains its linear-in-parameter form.

REFERENCES

[1] E. Ohnishi, I. Tsuboi, and T. Egusa, "Automatic control of an overhead crane," in *1981IFAC World Congress*, Kyoto, Japan, pp. 1885–1890.

[2] A. J. Ridout, "New feedback control system for overhead cranes," in *Proc. Electric Energy Conf.*, Adelaide, Australia, 1987, pp. 135–140.

[3] J. Yu, F. L. Lewis, and T. Huang, "Nonlinear feedback control of a gantry crane," in *Proc. American Control Conf.*, 1995, pp. 4310–4315.

[4] S. Garrido, M. Abderrahmin, A. Gimenez, R. Diez, and C. Balaguer, "Anti-swinging input shaping control of an automatic construction crane," *IEEE Trans. Autom. Sci. Eng.*, vol 5, no. 3, pp. 549–557, Jul. 2008.

[5] A. Piazzi and A. Visioli, "Optimal dynamic-inversion-based control of an overhead crane," *Proc. Inst. Elect. Eng. —Control Theory Appl.*, vol. 149, no. 5, pp. 405–411, Sep. 2002.

[6] Y. Fang, W. Dixon, D. Dawson, and E. Zergeroglu, "Nonlinear coupling control laws for an underactuated overhead crane System," *IEEE/ASME Trans. Mechatronics*, vol. 8, no. 3, pp. 418–424, Sep. 2003.

[7] N. Sun, Y.Fang, and X. Zhang, "A novel nonlinear coupling control approach for overhead crane: theory and implementation," in *Proc. American Control Conf.*, Montreal, Canada, 2012, pp. 6276–6281.

[8] D. Chwa, "Nonlinear tracking control of 3-D overhead crane against the initial swing angle and the variation of payload weight," *IEEE Trans. Control Syst. Technol.*, vol. 17, no. 4, pp. 876–883, Jul. 2009.

[9] H. H. Lee, "A new design approach for the anti-swing control of overhead cranes with high-speed load hoisting," *Int. J. Control*, vol. 77, no. 10, pp. 931–940, Jul. 2004.

[10] Y. Fang, B. Ma, P. Wang, and X. Zhang, "A motion planning-based adaptive control method for an underactuated crane system," *IEEE Trans. Control Syst. Technol.*, vol. 20, no. 1, pp. 241–248, Jan. 2012.

[11] H. Yang and K. S. Yang, "Adaptive coupling control for overhead crane systems," in *Proc. American Control Conf.*, Minneapolis, MN, USA, 2006, pp. 1832–1837.

[12] C. Vazquez, L. Fridman, and J. Collado, "Second order sliding mode control of a 3-dimensional overhead crane," in *Proc. 51st IEEE Conf. Decis. Control*, Hawaii, USA, 2012, pp. 6472–6476.

[13] H. H. Lee, Y. Liang, and D. Segura, "A sliding-mode antiswing trajectory control for overhead cranes with high-speed load hoisting," *ASME J. Dyn. Syst. Meas. Control*, vol. 128, pp. 842–845, Dec. 2006.

[14] C. Y. Chang, "Adaptive fuzzy controller of the overhead cranes with nonlinear disturbance," *IEEE Trans. Indus. Info.*, vol. 3, no. 2, pp. 164–172, May 2007.

[15] Y. Zhao and H. Gao, "Fuzzy-model-based control of an overhead crane with input delay and actuator saturation," *IEEE Trans. Fuzzy Syst.*, vol. 20, no. 1, pp. 181–186, Feb. 2012.

[16] M.Vukov, W. V. Loock, B. Houska, H. J. Ferreau, J. Swevers, and M. Diehl, "Experimental validation of nonlinear MPC on an overhead crane using automatic code generation," in *Proc. American Control Conf.*, Montreal, Canada, 2012, pp. 6264–6269.

[17] B. Kapernick and K. Graichen, "Model predictive control of an overhead crane using constraint substitution," in *Proc. American Control Conf.*, Washington, DC, USA, 2013, pp. 3973–3978.

[18] C. Y. Chang, H. W. Lie, "Real-time visual tracking and measurement to control fast dynamics of overhead cranes," *IEEE Trans. Indus. Electro.*, vol. 59, no. 3, pp. 1640-1649, Mar. 2012.

[19] Z. Xi and T. Hesketh, "Discrete time integral sliding mode control for overhead crane with uncertainties," J. *IET Control Theory Appl*, vol. 4, no. 10, pp. 2071–2081, Oct. 2010.

[20] M. W. Spong, S. Hutchinson, and M. Vidyasagar, *Robot Modeling and Control*. Hoboken, NJ: John Wiley and Sons, 2006.

[21] F. L. Lewis, D. M. Dawson, and C. T. Abdallah, *Robot Manipulator Control: Theory and Practice*. 2nd ed. New York, NY: Marcel Dekker, 2004.

[22] H. H. Lee, "Motion planning for three-dimensional overhead cranes with high-speed load hoisting," *Int. J. Control*, vol. 78, no. 12, pp. 875–886, Aug. 2005.

[23] H. H. Lee, "Modeling and control of a three-dimensional overhead crane," *ASME J. Dyn. Syst. Meas. Control*, vol. 120, pp. 471–476, 1998.

[24] A. Khatamianfar, "A new approach to overhead cranes parameter estimation and friction modeling," *in Proc*. 2014 *IEEE Int. Conf. Syst*., *Man and Cybern*., *SMC2014*, San Diego, CA, USA, 2014, pp. 2581–2586.

[25] K. J. Astrem and B. Wittenmark, *Computer-Controlled Systems*. 3rded. Upper Saddle River, NJ: Prentice Hall, 1997.

[26] C. Canudas, K. J. Astrom, and K. Braun, "Adaptive friction compensation in DC-motor drives," *IEEE J. Robot. Autom.*, vol. 3, no. 6, December 1987.

[27] H. K. Khalil, *Nonlinear systems*. 3rd ed. Englewood Cliffs, NJ: Prentice-Hall, 2002.

[28] R. E. Kalman and J. E. Bertram, "Control system analysis and design via the second method of Lyapunov-II—discrete-time systems," *J. Basic Eng.-Trans. ASME*, vol. 82, no. 2, pp. 394–400, Jun. 1960.

[29] INTEGO Limited, Poland, http://www.inteco.com.pl.

[30] J. Kautsky, N. K. Nichols, and P V. Dooren, "Robust pole assignment in linear state feedback," *Int. J. Control*, vol. 41, no. 5, pp. 1129–1155, 1985.